

# Curvature Effects in Gamma-Ray Bursts

A. Shenoy,<sup>1</sup> E. Sonbas,<sup>2,3</sup> C. Dermer,<sup>4</sup> L. C. Maximon,<sup>1</sup> K. S. Dhuga,<sup>1</sup>  
P. N. Bhat,<sup>5</sup> J. Hakkila,<sup>6</sup> W. C. Parke,<sup>1</sup> G. Maclachlan,<sup>1</sup> T. N. Ukwatta.<sup>7</sup>

<sup>1</sup>Department of Physics, The George Washington University  
Washington, D.C. 20052, USA

<sup>2</sup>Department of Physics, University of Adiyaman  
02040, Adiyaman, Turkey

<sup>3</sup>NASA Goddard Space Flight Center  
Greenbelt, MD 20771, USA

<sup>4</sup>Space Science Division, Code 7653, Naval Research Laboratory  
Washington, D.C. 20375, USA

<sup>5</sup>CSPAR, University of Alabama in Huntsville  
Huntsville, AL 35805, USA

<sup>6</sup>Department of Physics and Astronomy, College of Charleston  
Charleston, S.C. 29424, USA

<sup>7</sup>Department of Physics and Astronomy, Michigan State University  
East Lansing, MI 48824, USA

E-mail: ashwinsp469@gmail.com, edasonbas@yahoo.com, charles.dermer@nrl.navy.mil  
max@gwu.edu, dhuga@gwu.edu, Narayana.Bhat@nasa.gov, hakkilaj@cofc.edu,  
wparke@gwu.edu, maclach@gwu.edu, tilan.ukwatta@gmail.com

April 16, 2013

## Abstract

Curvature effects in Gamma-ray bursts (GRBs) have long been a source of considerable interest. In a collimated relativistic GRB jet, photons that are off-axis relative to the observer arrive at later times than on-axis photons and are also expected to be spectrally softer. In this work, we invoke a relatively simple kinematic two-shell collision model for a uniform jet profile and compare its predictions to GRB prompt-emission data for observations that have been attributed to curvature effects such as for the peak-flux–peak-frequency relation, i.e., the relation between the  $\nu F_\nu$  flux and the spectral peak,  $E_{peak}$  in the decay phase of a GRB pulse, and spectral lags. We present the case of the single-pulse Fermi GRB 110920, as a test for the predictions of the model against observations.

# 1 Introduction

Pulses in GRB light curves are thought to be produced by collisions between relativistic shells ejected from an active central engine (Rees and Meszaros 1994). The interception of a more slowly moving shell by a second shell that is ejected at a later time, but with faster speed, produces a shock that dissipates internal energy to accelerate the particles that emit the GRB radiation. This scenario is widely adopted in order to model pulses in GRB light curves (e.g., Daigne and Mochkovitch 1998; Zhang et al. 2009). Studies of pulses are important to decide if GRB sources require engines that are long-lasting or impulsive, and to determine the likely radiation mechanism(s), with important implications for the nature of the central engine.

Spectral lags, where low energy photons reach the observer at later times than high-energy photons, are seen in a significant fraction of GRBs. Cheng et al. (1995) were the first to analyze the spectral lag of GRBs, which they determined as the time delay between the peaks in the Burst and Transient Source Experiment (BATSE) Large Area Detector (LAD) channel 1 (25 - 50 keV) and channel 3 (100 - 300 keV) light curves. Since then, several authors have analyzed spectral lags in GRBs, while also extending these observations to the Swift and Fermi GRB samples (e.g., Norris et al. 1996; Norris, Marani & Bonnell 2000, Wu & Fenimore 2000; Chen et al. 2005; Ukwatta et al. 2010a). The leading model to explain the spectral lag is the curvature effect, i.e. the kinematic effect due to the observer looking at an increasingly off-axis annulus area relative to the line-of-sight (Salmonson 2000; Ioka and Nakamura 2001; Shen et al. 2005; Lu et al. 2006). Softer low-energy radiation comes from the off-axis annulus area due to smaller Doppler factors. This radiation is also delayed at the observer end with respect to on-axis observation due to the geometric curvature of the shell.

Both the existing models and observations suggest that a connection exists between the observed hard-to-soft spectral evolution of GRB pulses and spectral lags. It is therefore important to understand the mechanism that produces this evolution. Tavani (1996) proposed that this hard-to-soft spectral evolution is caused by the variation of the average Lorentz factor of pre-accelerated particles and the strength of the local magnetic field at the GRB site as the synchrotron emission evolves within the burst. Liang (1997) proposed a physical model of hard-to-soft spectral evolution in which impulsively accelerated non-thermal leptons cool by saturated Compton up-scattering of soft photons. Kocevski & Liang (2003) have pointed out that the nature of hard-to-soft spectral evolution is a difficult issue to address due to uncertainties involved with the microphysics of GRBs. They analyzed a sample of 19 GRBs, and found an empirical relation between the decay rate of the peak energy and the GRB lag. Ukwatta et al. (2010a) have analyzed a sample of 31 Swift GRBs with known red-shifts and determined that the source-frame  $E_{peak}$  lies outside the energy band 100 – 250 keV for a majority of bursts, suggesting that spectral evolution may not be the dominant process causing the observed spectral lag.

Borgonovo and Ryde (2001) studied the spectral evolution in the prompt-emission in GRBs by performing a time-resolved spectral analysis of BATSE single pulses and showed that in many cases the  $\nu F\nu$  flux at the  $E_{peak}$ ,  $f_{E_{pk}}$ , for each time segment was  $\propto E_{peak}^\eta$  (hereafter referred to as the peak-flux–peak-frequency relation), with  $\eta$

Table 1: Selected parameters for the generation of the model light curves unless otherwise stated.

$\eta_r$	$\eta_t$	$\eta_\Delta$	$t_{var}(secs)$	$\Gamma$	$z$	$\theta_{jet}$	$E_{pk,0}$ (keV)	$d_L$ (cm)	$u_0$ (ergs cm $^{-3}$ )
1.0	1.0	1.0	1.0	300	1.0	4.0/ $\Gamma$	250.0	$2.2 \times 10^{28}$	1.0

ranging from  $\approx 0.6$  to 3. The exponent  $\eta$  was found to stay roughly constant for pulses within the same GRB. Dermer (2004) modeled and analyzed GRB pulses based on curvature effects with a Broken-Power-Law (BPL) intrinsic spectrum and showed that in the curvature limit,  $\eta$  was equal to 3 for pulses with a wide range of temporal properties. He concluded on the basis of the Borghonovo and Ryde result that curvature effects do not play a prominent role in GRB prompt-emission.

While several studies (Qin et al. 2003; 2004; Shen et al. 2005; Lu et al. 2005) have been performed to determine the role played by curvature effects, both in the spectral evolution of GRB prompt-emission as well as in producing spectral lags, many questions remain unanswered. An intriguing result connected to lag observations is the lag-luminosity anti-correlation (see Norris et al. 2000; Ukwatta et. al 2010a). This anti-correlation is further evidence for a connection between lags and the mechanism(s) that drive the GRB.

In this paper, we investigate the effects of curvature by comparing the behavior of selective temporal and spectral characteristics of GRB prompt emission with the predictions of a simple two-shell collision model. The paper is organized as follows: the basic features of the model are presented in section 1.1, followed by a description of the sample selection criteria, analysis methodology, and a case study in section 2. The discussion of our main results is presented in section 3, followed by a brief summary of our conclusions in section 4.

## 1.1 The Model

We have used a particular representation of the internal shock model for our purposes (Dermer 2004). This model consists of a single two-shell collision event occurring at a radius  $r_0$  from the source, generating a uniform spherical shell, with Lorentz factor  $\Gamma$ , that radiates for a co-moving time between  $t'_0$  and  $t'_0 + \Delta t'$  with  $\Delta t' = \eta_\Delta \Gamma t_{var}/(1+z)$ . where  $t_{var}$  is the observed variability time scale. The intrinsic-emission profile is assumed to be rectangular with instantaneous rise and decay phases. The co-moving width of this shell  $\Delta r'$  is assumed to remain constant during the period of illumination and given by  $\Delta r' = \eta_\Delta \Gamma c t_{var}/(1+z)$ . The emission spectrum in the co-moving frame may be described by any suitable spectral function such as, a Broken Power-Law (BPL), Band or Comptonized- $E_{peak}$ , peaking at a co-moving photon energy  $E'_{pk,0} = (1+z) E_{pk,0}/2\Gamma$  where  $E_{pk,0}$  is the observer frame  $E_{pk}$  at the start of the pulse. The spectral indices at  $E < E_{pk,0}$  and at  $E > E_{pk,0}$  in counts space are denoted  $\alpha$  and  $\beta$ , respectively. The curvature constraint requires that  $r \lesssim 2\Gamma^2 c t_{var}/(1+z)$  (see Dermer 2004 and references therein). The radius is thus written using the expression  $r_0 = 2\eta_r \Gamma^2 c t_{var}/(1+z)$ , with  $0 \lesssim \eta_r \lesssim 1$ . The parameters  $\eta_t$ ,  $\eta_\Delta$  and  $\eta_r$  thus control the blast-wave duration, shell-thickness and radius of emission respectively.

Unless otherwise stated, the selected parameters used for the numerical calculations

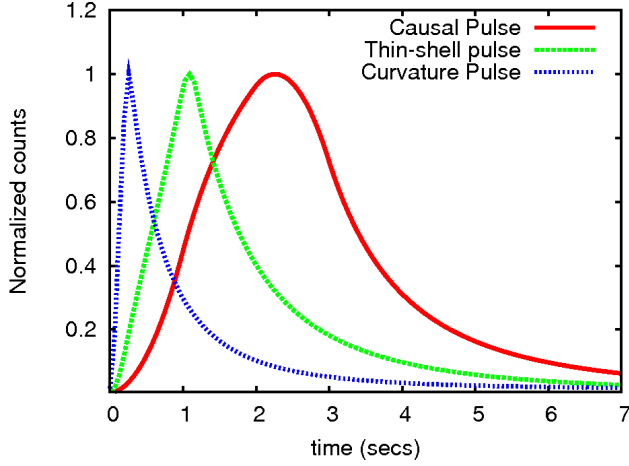


Figure 1: Normalized light curves obtained using selected parameters except: Thin-shell pulse,  $\eta_\Delta = 0.1$ ; and the Curvature pulse,  $\eta_\Delta = \eta_t = 0.1$ . The case of  $\eta_t = \eta_\Delta = \eta_r = 1$  is referred to as a Causal pulse (see Dermer 2004 for a detailed discussion of these three generic types of pulses).

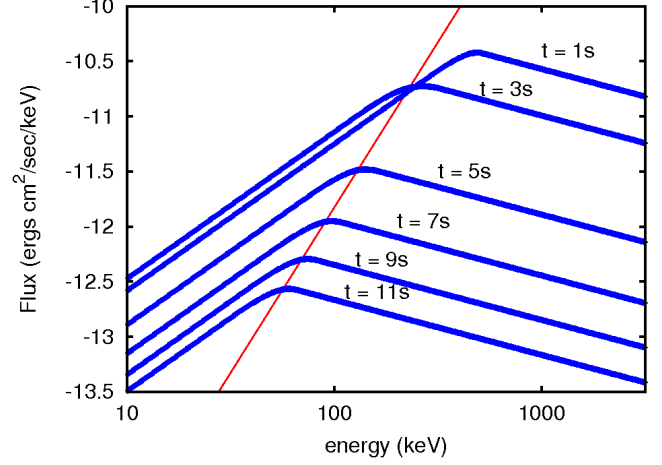


Figure 2: Evolution of the spectral energy distribution due to curvature effects for the case of the causal pulse in Fig. 1. In the declining phase of the pulse, the value of  $f_{\epsilon_{pk}} \propto \epsilon_{pk}^3$ , as shown by the red line.

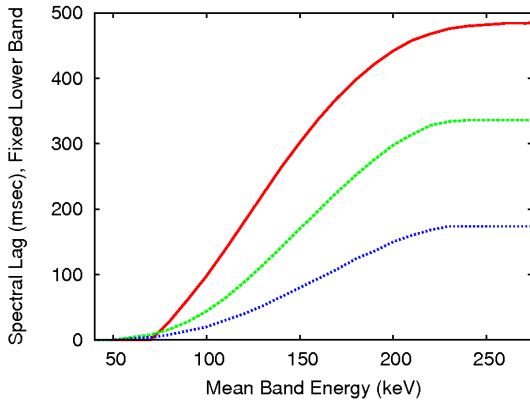


Figure 3: Lag vs. Energy for selected parameters shell thickness  $\eta_\Delta$ . Red:  $\eta_\Delta = 1.0 c\Delta t'$ ; Green:  $\eta_\Delta = 0.5 c\Delta t'$ ; Blue:  $\eta_\Delta = 0.1 c\Delta t'$ .

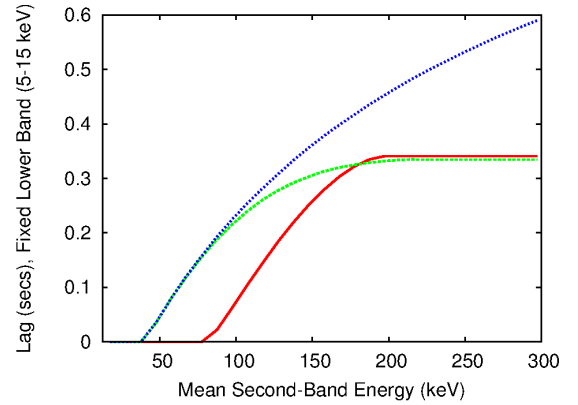


Figure 4: Lag vs. Energy due to different intrinsic spectral functions with selected parameters except  $E_{pk,0} = 200$  keV. Here, Red: Broken-power-law with  $\alpha = -2/3$ ,  $\beta = -2.5$ , Green: Band function with  $\alpha = -0.8$ ,  $\beta = -2.25$  and Blue: Comptonized- $E_{peak}$  with  $\alpha = -0.8$ .

of the light curves, spectra and spectral lags are shown in Table. 1. Fig. 1 shows the normalized, generic pulse shapes obtained using the selected parameters. Fig. 2 shows the evolution of the spectral energy distribution for the case of the curvature pulse shown in Fig. 1. The  $\nu F_\nu$  peak flux  $f_{E_{pk}} \propto E_{pk}^3$  equality line is shown in the decay portion of the pulse. Dermer (2004) shows that this equality holds in the declining phase for all pulses. Fig. 3 shows the spectral lag as a function of energy for a case with selected parameters but with varying shell thickness,  $\eta_\Delta$ . For a broken-power-law intrinsic spectrum, the lag shows a relatively well-defined "S-shaped" trend with no lags at energies below  $\sim 0.3E_{pk,0}$  and no lags for all energies above  $E_{pk,0}$ . Increasing or decreasing the value of  $E_{pk,0}$ , while keeping all other model parameters fixed, only shifts the entire curve in the direction of increase or decrease. Shen et al. (2005) studied the lags due to curvature effects using different intrinsic emission profiles. They found that for an infinitesimal shell, a rectangular profile produces no lags. We find that the situation is quite different for the case of a finite shell thickness. Fig. 4 shows the lag as a function of energy for a case with selected parameters but with different intrinsic spectral functions (BPL, Band, and Comptonized- $E_{peak}$ ). It is seen that a change in the intrinsic spectrum has a significant effect in the evolution of the spectral lag with energy. In the case of a Band or Comptonized- $E_{peak}$  function, the lags are small for energies small compared to  $E_{pk,0}$ , and that the lags for a Comptonized- $E_{peak}$  function do not show a saturation energy. This is because the Comptonized- $E_{peak}$  function varies monotonically at all energies and does not have a well-defined break energy.

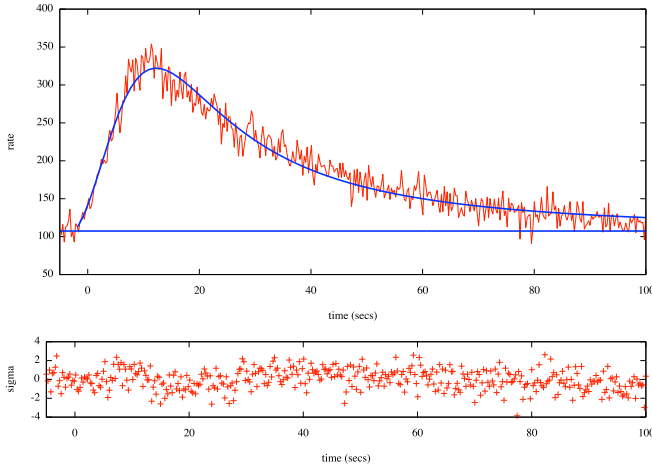


Figure 5: KRL pulse-fit for the light curve for GRB 110920 with residuals.

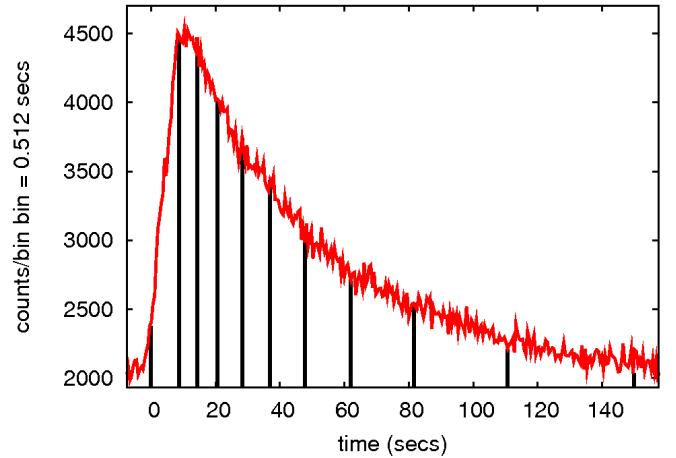


Figure 6: Light curve segments for 110920 with equal fluences.

## 2 Sample Selection and Methodology.

The model assumes that pulses in GRBs are produced by single two-shell-collision events. As a first step we therefore analyze either single-pulse GRBs, or GRBs with relatively simple light curves where the individual pulses within a multi-pulse structure in the light curve can be distinguished. In addition, we require that the GRB pulses be bright enough and of sufficient duration (the duration of the pulse is particularly

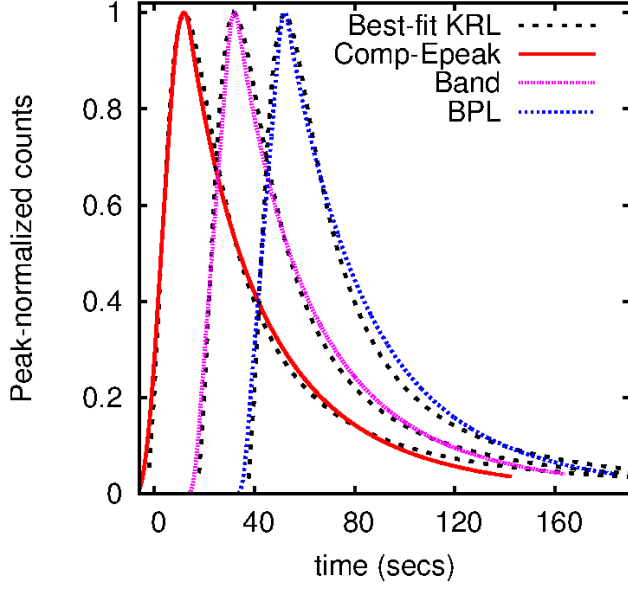


Figure 7: Comparable pulses generated using the BPL ( $E_{peak} = 300$  keV,  $\alpha = \frac{4}{3}$ ,  $\beta = -\frac{1}{2}$ ), Band ( $E_{peak} = 334$  keV,  $\alpha = -0.2$ ,  $\beta = -2.65$ ) and Comptonized- $E_{peak}$  ( $E_{peak} = 280.1$  keV,  $\alpha = -0.46$ ) spectral functions. The light curves have been offset by 20 seconds for better viewing.

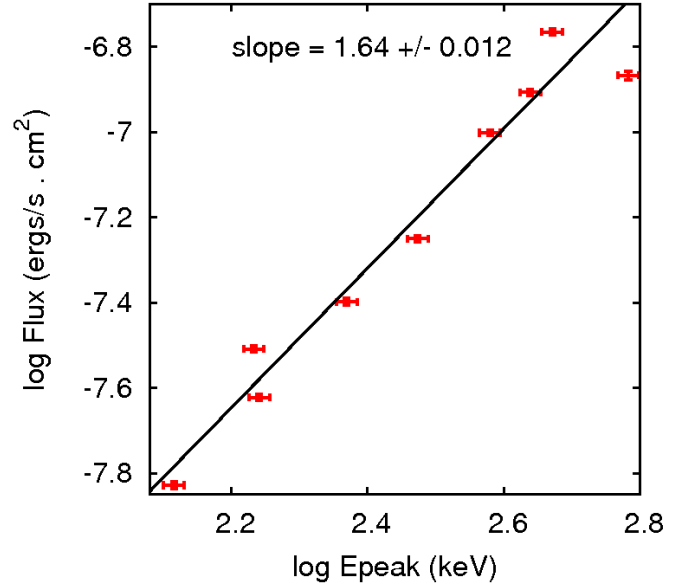


Figure 8:  $\nu F\nu$  Flux vs.  $E_{peak}$  for the data from GRB 110920. The data were fit with the best-fit Comptonized- $E_{peak}$  function in the range 100-985 keV.

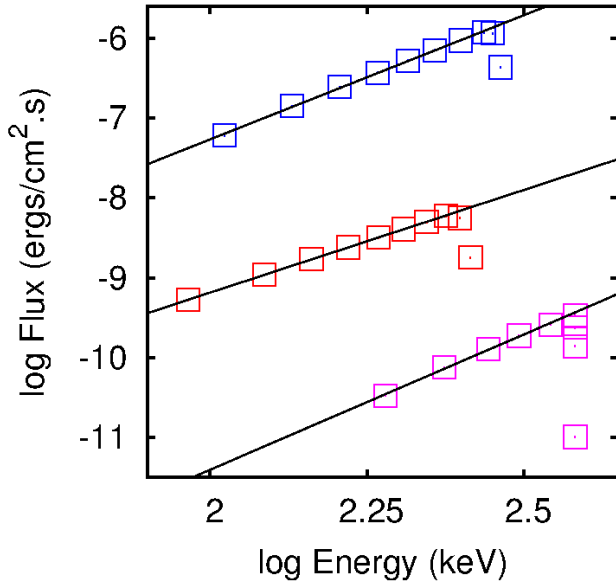


Figure 9:  $\nu F\nu$  Flux vs.  $E_{peak}$  from the model for the three intrinsic spectral functions described in the text with Blue: BPL; slope =  $3.11 \pm 0.04$ , Pink: Band; slope =  $3.39 \pm 0.10$  and Black: Comptonized- $E_{peak}$ ; slope =  $2.57 \pm 0.01$ , for time segments identical to those used for the data. The flux scale has been offset for better viewing.

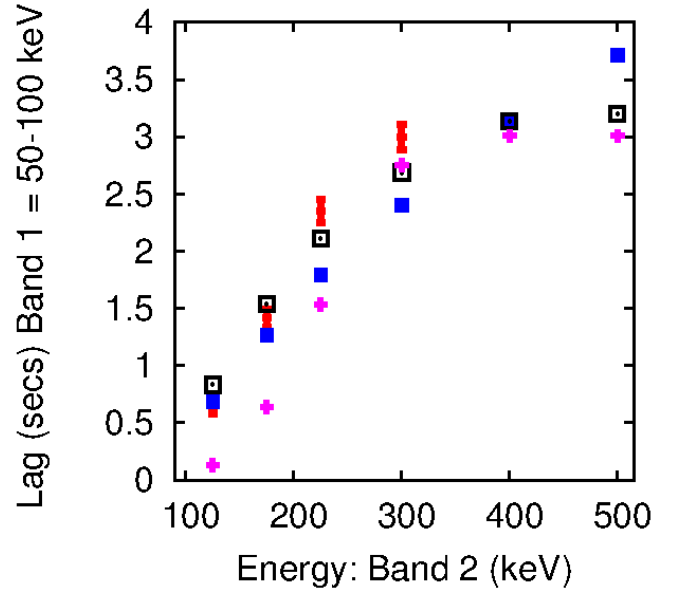


Figure 10: Lag vs. energy from the model for the pulses shown in Fig. 7 with Red: Data, Solid blue squares: Comptonized- $E_{peak}$ , Hollow black squares: Band function and Pink crosses: BPL. The Band 2 energies are the mid-point of the energy in the second band.

relevant to tests of the peak-flux – peak-frequency relation) so that we may obtain reliable results from our analyses.

After identifying a potential candidate GRB, we pulse-fit the GRB light curves using a suitable pulse function (such as the Kocevski-Ryde-Liang (KRL) pulse function: see Kocevski Ryde & Liang 2003 or the Norris pulse function: see Norris et al. 2004) in multiple energy bands and then make a determination of the suitability of the GRB for our analyses. In order to confirm whether a given pulse (obtained from a suitable pulse-fit) is indeed a single pulse within statistics, we perform a wavelet based minimum-variability time-scale (MTS) extraction. The connection between pulses and the MTS has been established by MacLachlan et al. (2012). The best-fit pulse profile is then used as a representation of the light curve from the data.

The time-integrated spectrum of the GRB is fit with a suitable function (Band, Comptonized- $E_{peak}$  etc.). The best-fit spectral function is used as the intrinsic emission spectrum in the model. The model parameters are then varied to generate a light curve that best matches the best-fit pulse profile. The light curve is subdivided into time segments and an  $E_{peak}$  is extracted via a spectral fit for each time segment. The  $\nu F_\nu$  flux is extracted around  $E_{peak}$ . The model light curve is treated in an identical fashion as the data with regard to segments. Model fluxes and  $E_{peak}$ 's are extracted and the peak-flux – peak-frequency relation is tested. Independent of this test, we also extract spectral lags in suitable, identical energy bands from the data and the model and compare the predicted and the observed spectral-lag-energy evolution. The spectral lags are extracted using the cross-correlation function (CCF) analysis method as described in Ukwatta et. al (2010).

## 2.1 GRB 110920 - A Test Case

The Fermi GRB 110920 is a single-pulse burst with a relatively long fast rise, exponential decay (FRED) structure with a  $T_{90}$  of  $170 \pm 17$  seconds. The best fit Band parameters (see McGlynn et al. 2012 for a detailed discussion on the properties of this GRB) for the time interval  $[T_0 + 0.003, T_0 + 52.737]$  (where  $T_0$  is the trigger time) were  $\alpha = -0.20 \pm 0.02$ ,  $\beta = -2.65^{+0.07}_{-0.09}$  and  $E_{peak} = 334 \pm 5$  keV with C-stat = 3206.5 (485 d.o.f.). However, when a blackbody component was included in the fit, the C-stat was reduced to 2848.3 (483 d.o.f.). The peak energy of the Band component was shifted up to  $E_{peak} = 978^{+154}_{-121}$  keV and the temperature of the blackbody was found to be  $kT = 61.3^{+0.7}_{-0.6}$  keV. The low energy index  $\alpha$  became shallower ( $-1.05 \pm 0.04$ ). McGlynn et al. (2012) have attributed this blackbody component to the photospheric emission (see for instance: Ryde, 2005; Rees & Meszaros, 2005). Since the redshift ( $z$ ) is undetermined for this GRB, they have assumed a value of  $z = 2$  and then used photospheric emission models to obtain a bulk Lorentz factor of  $\sim 440$ .

The persistence of the soft component at late times made initial attempts to pulse-fit the light curve rather difficult. A careful analysis, based partly on the results presented above, allowed us to separate the underlying pulse structure from the overall structure of the light curve. Fig. 5 shows the full light curve for the GRB in the energy range 100

– 985 keV along with the best-fit KRL pulse function. The energy range was so chosen to avoid contamination from the soft component (below 100 keV). Once this was done, the parameters obtained from the KRL pulse-fits in different energy bands showed a consistent pattern in terms of their values, as well as the degree of correlation between them. The MTS we extracted for this light curve is about 1.3 seconds, thus suggesting that this GRB is most likely a single-pulse GRB with no additional structures.

The best-fit KRL function was then used as the representation of the light curve to be matched by the model. We assumed a Bulk Lorentz factor  $\Gamma$  of 440 and  $z = 2$  (identical to McGlynn et al. 2012). With these parameters, we extract a radius,  $r_0$  of about  $10^{17}$  cm from the model. Fig. 6 shows the segmentation of the light curve into equal-fluence segments. The time-resolved energy-spectrum of the pulse was fit with a Band function (identical to McGlynn et al 2012, in the energy range, 8 - 985 keV) and a Comptonized- $E_{peak}$  function (in the range 100-985 keV) and these, along with a theoretical BPL function (originally used by Dermer 2004) were used as intrinsic spectra for the model. With a suitable choice of shell-collision parameters, we extracted best-fit pulses using these three spectral functions (see Fig. 7 for the pulses as well as details of the corresponding spectral parameters). Figs. 8 and 9 show our results for the peak-flux–peak-frequency for the data with the best-fit Comptonized- $E_{peak}$  function and the model using the three different intrinsic spectra. Fig. 10 shows the spectral lags for the light curves of Fig. 7.

### 3 Discussion

The above results show that an internal shock model with an intrinsic spectrum identical to that used to fit the data (the Comptonized- $E_{peak}$  and Band functions), reproduces the observed pulse profile as well as the observed spectral lags. It was difficult to determine if there was a saturation energy present in the lag-energy-evolution (Fig. 10) as there were insufficient counts to extract lags in higher energy bands. As noted earlier, a finite shell thickness can account for observed lags even for the case of a rectangular intrinsic emission profile. A second Band function component with a peak shifted to 1 MeV (when a blackbody component is included in the fit) would imply a 1 MeV break energy in the lag-energy plot, and would also predict no lags (or small lags in the case of the Comptonized- $E_{peak}$ ) below  $\sim 300$  keV. This does not match the observations. It can be seen from Fig. 9 that the exponent in the peak-flux–peak-frequency relation is close to 3 in all cases for the model pulses shown in Fig. 7. This confirms the observations of Dermer (2004) that the exponent at times after the peak of the light curve is close to 3 even with different choices of intrinsic spectra. However, this does not match the exponent obtained from the data (Fig. 8). This further supports the conclusions of Dermer (2004) that curvature alone cannot account for the spectral evolution seen in GRB prompt-emission. While a connection may exist between the observed spectral evolution and the spectral lags, it appears that curvature effects alone cannot describe this connection and additional emission mechanisms may be needed. We note in passing that Guirec et al. (2012) have shown that the inclusion of a blackbody component in the spectral fits leads to an improved description of the spectral properties of a number of GRBs.



## 4 Conclusions

We have used a simple two-shell collision model to investigate curvature effects in the prompt emission of GRBs. In addition to the BPL for the intrinsic-emission spectrum used in Dermer (2004), we have also examined the effects of using other emission spectra such as the Band, and the Comptonized- $E_{peak}$  functions. In this study, we focused primarily on the peak-flux – peak-frequency relation which is predicted to have a power-law behavior with an exponent of 3, and the energy evolution of spectral lags. We compare our model results with the results of similar models in the literature and also present a test case study of GRB 110920.

We summarize our main findings as follows:

- While we agree with Shen et al (2005) that an infinitesimal shell produces no discernible spectral lag using a rectangular emission-pulse-profile, we find the situation to be different for a shell of finite thickness i.e., a finite spectral lag can be produced even with a rectangular pulse profile;
- The spectral lag evolution as a function of energy is quite sensitive to the type of intrinsic spectrum. For example, the Comptonized- $E_{peak}$  model does not appear to exhibit a saturation energy at which the spectral lags reach a plateau phase as in the case of the Band and the broken-power-law functions. We agree with Shen et al (2005) that the spectral lags seem to approach a maximum when  $E_{peak}$  is near the high-energy channel used in extracting the lag. Most likely this simply reflects the break energy present in the assumed intrinsic spectrum (i.e., Band and BPL);
- All intrinsic spectral models tested exhibit the peak-flux – peak-frequency relation although with exponents that differ from the predicted exponent of 3. The significance of this discrepancy is not clear at this stage and warrants further investigation;
- The peak-flux – peak-frequency test for GRB 110920 yields an exponent of  $1.64 \pm 0.012$  compared to the theoretical one of  $2.57 \pm 0.01$  (with Comptonized- $E_{peak}$  as the intrinsic spectrum). We consider this discrepancy to be significant and the result to be in disagreement with the prediction based purely on effects of curvature. Similar conclusions were reached by Dermer (2004) and Borgonovo and Ryde (2001);
- Relatively good agreement is obtained with all intrinsic spectral models for the spectral lag versus energy for GRB 110920. This is somewhat surprising given the result stated in the previous bullet. It is possible that this result is due to the interplay between model parameters such as shell thickness, variability time scale, the energy evolution of  $E_{peak}$  and the Lorentz factor. The investigation of the dependencies of these various parameters is ongoing.

We note that the role of the reported soft component of the light curve for GRB 110920 has not been fully investigated in this study and is worth pursuing, particularly

with regard to the behavior of the peak-flux–peak-frequency relation. Finally, we note that these studies are being extended to a larger sample of GRBs.

## 5 References

- Borgonovo, L. & Ryde, F. 2001, *ApJ*, 548, 770  
 Chen L., et al., 2005, *ApJ*, 619, 983  
 Cheng L. et al., 1995, *A&A*, 300, 746  
 Daigne F. & Mochkovitch, R. 1998, *MNRAS*, 296, 275  
 Dermer C. D. 2004, *ApJ*, 614, 284  
 Fenimore E. E., Madras, C. D., & Nayakshin, S. 1996, *ApJ*, 473, 998  
 Guirec S. et al., 2012, 2012arXiv1210.7252G  
 Ioka K., Nakamura T., 2001, *ApJ*, 554, L163  
 Kocevski D., Liang E., 2003, *ApJ*, 594, 385  
 Kocevski D., Ryde F., & Liang E., 2003, *APJ*, 596, 389  
 Liang E. P., 1997, *ApJ*, 491, L15  
 Lu R.-J., et al., 2006, *MNRAS*, 367, 275  
 Maclachlan G. et al., 2012, *MNRAS*, 425, L32  
 McGlynn S. et al., *PoS, GRB2012* (2012)  
 Norris J. P. et al., 1996, *ApJ*, 459, 393  
 Norris J. P., Marani G. F., Bonnell J. T., 2000, *ApJ*, 534, 248  
 Norris, J. P. et al. 2005, *ApJ* 627, 324  
 Qin Y.-P., et al., 2003, *A&A*, 407, 393  
 Qin Y.-P., et al., 2004, *ApJ*, 617, 439  
 Rees, M. J., Meszaros, P. 1994, *ApJ*, vol. 430, p. L93  
 Ryde F., 2005, *ApJ* 625, L95  
 Rees M. J., and Meszaros P., 2005, *ApJ* 628, 847  
 Salmonson J. D., 2000, *ApJ*, 544, L115  
 Shen, R-F., Song L-M., Zhuo L., 2005, *MNRAS*, 362, 59  
 Tavani, M., 1996, *ApJ*, 466, 768  
 Ukwatta, T. N. et al., 2010a, *MNRAS*, 711, 1073  
 Wu B., Fenimore E., 2000, *ApJ*, 535, L29  
 Zhang, B.-B. et al., 2009, *ApJ*, 690, L10